Energy &
Environmental
Science

COMMUNICATION

View Article Online
View Journal | View Issue

Open Access Article. Published on 19 July 2016. Downloaded on 9/12/2024 7:48:15 PM.
This article is licensed under a Creative Commons Attribution-NonCommercial 3.0 Unported Licence.

Cite this: *Energy Environ. Sci.*, 2016, **9**, 2789

Received 21st June 2016,
Accepted 19th July 2016

DOI: 10.1039/c6ee01786j

www.rsc.org/ees

Engineering water dissociation sites in MoS_2 nanosheets for accelerated electrocatalytic hydrogen production†

Jian Zhang,[a] Tao Wang,[b] Pan Liu,[cd] Shaohua Liu,[a] Renhao Dong,[a] Xiaodong Zhuang,[a] Mingwei Chen[cd] and Xinliang Feng*[a]

Earth-abundant MoS_2 is widely reported as a promising HER electrocatalyst in acidic solutions, but it exhibits extremely poor HER activities in alkaline media due to the slow water dissociation process. Here we present a combined theoretical and experimental approach to improve the sluggish HER kinetics of MoS_2 electrocatalysts through engineering the water dissociation sites by doping Ni atoms into MoS_2 nanosheets. The Ni sites thus introduced can effectively reduce the kinetic energy barrier of the initial water-dissociation step and facilitate the desorption of the ^{-}OH that are formed. As a result, the developed Ni-doped MoS_2 nanosheets (Ni-MoS_2) show an extremely low HER overpotential of ~98 mV at 10 mA cm^{-2} in 1 M KOH aqueous solution, which is superior to those (>220 mV at 10 mA cm^{-2}) of reported MoS_2 electrocatalysts.

Broader context

Enhancing the sluggish kinetics of the electrocatalytic hydrogen evolution reaction (HER) in water–alkali electrolyzers is pivotal for large-scale and sustainable hydrogen production. Earth-abundant MoS_2 is widely reported as a promising HER electrocatalyst in acidic solutions, but it exhibits extremely poor HER activities in alkaline media due to the slow water dissociation process. Here we present a combined theoretical and experimental approach to improve the sluggish HER kinetics of MoS_2 electrocatalysts through engineering the water dissociation sites by doping Ni atoms into MoS_2 nanosheets. The Ni sites thus introduced can effectively reduce the kinetic energy barrier of the initial water-dissociation step and facilitate the desorption of the ^{-}OH intermediates that are formed. As a result, the developed Ni-doped MoS_2 nanosheets (Ni-MoS_2) show a highly competitive HER performance as compared to other state-of-the-art HER electrocatalysts. Therefore, this work opens up a favorable direction for exploring efficient and robust water-splitting electrocatalysts.

With its high energy density and environmentally friendly advantages, molecular hydrogen has been widely regarded as one of the most promising energy carriers.[1] The scalable and sustainable production of hydrogen fuel through efficient and cost-effective electrocatalytic/photocatalytic/photoelectrocatalytic water splitting technologies, *e.g.*, water–alkali and chlor-alkali electrolyzers, is highly promising as a means to meet the future global energy demands.[2] To this end, active, durable, and earth-abundant electrocatalysts are essential to lower the kinetic overpotentials of the hydrogen evolution reaction (HER) and ultimately accelerate hydrogen production in alkaline solutions.[3] Platinum (Pt) has been acknowledged as the most active and stable HER electrocatalyst with a near-zero onset overpotential.[4] Unfortunately, the large-scale utilization of Pt catalysts in H_2-production electrolyzers is seriously hampered by its scarcity and cost.

In regard to its elemental abundance, high activity, and electrochemical stability, molybdenum disulfide (MoS_2) is a promising catalyst for the electrocatalytic and photocatalytic HER.[5] Recently, both density functional theory (DFT) calculations and experimental results have demonstrated that the electrocatalytic HER activity of crystalline MoS_2 catalysts originates from the unsaturated Mo–S sites along the edges.[6] Inspired by this fundamental understanding, extensive efforts have been dedicated to increasing the number of exposed active sites on MoS_2 catalysts by engineering the nanostructures, *e.g.*, double-gyroid mesoporous MoS_2 films,[6] vertically aligned MoS_2 films,[8] defect-rich MoS_2 nanosheets,[9] amorphous MoS_x films,[10] $[Mo_3S_{13}]^{2-}$ clusters,[11] and CoS_x/MoS_x hybrids.[12] Unfortunately, although the MoS_2-based electrocatalysts thus developed exhibit enhanced HER activities in acidic solutions, the HER kinetics in alkaline electrolytes still suffer from a high overpotential (>220 mV at a current of 10 mA cm^{-2}).[12] The high kinetic energy barrier of

---

[a] *Center for Advancing Electronics Dresden (cfaed) & Department of Chemistry and Food Chemistry, Technische Universität Dresden, 01062 Dresden, Germany. E-mail: xinliang.feng@tu-dresden.de*

[b] *Université Lyon, Ens de Lyon, CNRS, Université Lyon 1, Laboratoire de Chimie, UMR 5182, F-69342, Lyon, France*

[c] *WPI Advanced Institute for Materials Research, Tohoku University, Sendai 980-8577, Japan*

[d] *CREST, JST, 4-1-8 Honcho Kawaguchi, Saitama 332-0012, Japan*

† Electronic supplementary information (ESI) available. See DOI: 10.1039/c6ee01786j

Open Access Article. Published on 19 July 2016. Downloaded on 9/12/2024 7:48:15 PM.
This article is licensed under a Creative Commons Attribution-NonCommercial 3.0 Unported Licence.

the initial water dissociation process (the Volmer step) and the strong adsorption of the formed ^{-}OH on the surfaces of MoS_2 are responsible for the sluggish HER kinetics in alkaline solutions.[13]

Herein, we demonstrate a novel strategy to efficiently speed up the sluggish HER kinetics of MoS_2 electrocatalysts through doping Ni atoms into crystalline MoS_2 nanosheets. The DFT calculations reveal the fact that the kinetic energy barrier of the initial water dissociation step and the adsorption interaction of ^{-}OH are substantially reduced on Ni-doped MoS_2 catalysts (Ni-MoS_2). Accordingly, Ni-MoS_2 nanosheets with a chemical composition of $Ni_{0.13}Mo_{0.87}S_2$ were prepared on carbon cloth *via* a one-pot hydrothermal reaction. The resultant Ni-MoS_2 nanosheets exhibit an excellent electrochemical HER activity in 1 M KOH aqueous solution with an extremely low overpotential of $\sim$98 mV at a current density of 10 mA cm^{-2}. The achieved overpotential is much lower than those of reported MoS_2 electrocatalysts (overpotential is $>$220 mV at 10 mA cm^{-2} in basic solutions and $\geq$110 mV at 10 mA cm^{-2} in acidic solutions).[12,14]

The kinetic energy barriers of the prior water dissociation step ($\Delta G(H_2O)$, Volmer step), the Gibbs free energy of adsorbed ^{-}OH (G(OH)), and the concomitant combination of H* intermediates into molecular hydrogen (ΔG(H), Tafel step) were firstly investigated using the DFT calculations according to the as-built catalyst models including MoS_2, Ni-MoS_2, Co-doped MoS_2 (Co-MoS_2), and Fe-doped MoS_2 (Fe-MoS_2) (Fig. S1, ESI†). As shown in Fig. 1 and Table S1 (ESI†), MoS_2 exhibits a very high $\Delta G(H_2O)$ up to 1.17 eV and an extremely low G(OH) (−5.24 eV). Substituting a Mo atom with a metal (Ni, Co, or Fe) atom along the edge of MoS_2 dramatically decreases the $\Delta G(H_2O)$ value in the order of: Ni-MoS_2 ($\Delta G(H_2O) = 0.66$ eV) $<$ Co-MoS_2 ($\Delta G(H_2O) = 0.76$ eV) $<$ Fe-MoS_2 ($\Delta G(H_2O) = 0.96$ eV). In contrast to MoS_2, the G(OH) value is reduced to −3.46 eV for Ni-MoS_2, −3.46 eV for Co-MoS_2, and −3.36 eV for Fe-MoS_2. These greatly reduced $\Delta G(H_2O)$ and G(OH) values on Ni-MoS_2 suggest that the kinetics of the initial water dissociation step and the concomitant desorption of the formed ^{-}OH can be effectively promoted after the doping of a Ni atom into the edge of MoS_2. In addition, the ΔG(H) is −0.06 eV for Ni-MoS_2, 0.13 eV for Co-MoS_2, and −0.10 eV for Fe-MoS_2, which are much lower than 0.60 eV for MoS_2. The negative value of ΔG(H) for Ni-MoS_2 catalysts shows that the subsequent Tafel step towards molecular hydrogen can spontaneously occur in thermodynamics.

Encouraged by these DFT results, we prepared metal-doped MoS_2 nanosheets (M-MoS_2), where the metal (Ni, Co, or Fe) atoms are homogeneously doped into the crystalline MoS_2 nanosheets, as schematically illustrated in Fig. S2 (ESI†). Specifically, the Ni-MoS_2 nanosheets were constructed on carbon cloth (1 × 3 cm^2) through a one-pot hydrothermal reaction at 200 °C for 24 h, involving $NiSO_4{\cdot}6H_2O$, $Na_2MoO_4{\cdot}2H_2O$, and L-cysteine in 15 mL deionized water. The molar content (x, expressed in $Ni_xMo_{1-x}S_2$) of Ni in the as-obtained Ni-MoS_2 nanosheets could be tuned from 6.2% to 19.1% by adjusting the dosage of $NiSO_4{\cdot}6H_2O$. The loading weight of Ni-MoS_2 nanosheets on the carbon cloth was approximately 0.89 mg cm^{-2}. Under the same hydrothermal conditions, Co-MoS_2 ($Co_{0.03}Mo_{0.97}S_2$) and Fe-MoS_2 ($Fe_{0.12}Mo_{0.88}S_2$) nanosheets on carbon cloth were also prepared utilizing $CoSO_4{\cdot}7H_2O$ and $FeSO_4{\cdot}7H_2O$ as Co and Fe sources, respectively. For comparison, pristine MoS_2 nanosheets were synthesized through the same process without involving $NiSO_4{\cdot}6H_2O$.

The crystalline structure of the M-MoS_2 nanosheets was first confirmed by X-ray diffraction (XRD) measurements. As shown in Fig. S3 (ESI†), the Ni-MoS_2 nanosheets show the diffraction peaks at diffraction angles similar to semiconducting MoS_2.[15] To probe the morphologies of the as-obtained Ni-MoS_2, scanning electron microscopy (SEM) and high-resolution transmission electron microscopy (HRTEM) were employed. Fig. 2a and Fig. S4 (ESI†) reveal numerous sheet-like nanostructures, which are vertically aligned and inter-connected on the carbon cloth. The thickness and length of the Ni-MoS_2 nanosheets are approximately 5–10 nm and 40–100 nm, respectively. Elemental mappings of

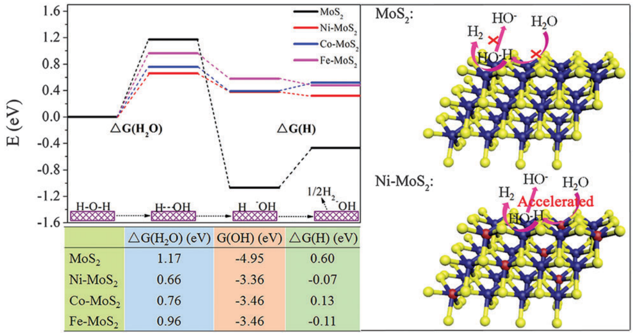

	△G(H₂O) (eV)	G(OH) (eV)	△G(H) (eV)
MoS₂	1.17	-4.95	0.60
Ni-MoS₂	0.66	-3.36	-0.07
Co-MoS₂	0.76	-3.46	0.13
Fe-MoS₂	0.96	-3.46	-0.11

Fig. 1 The results of the DFT calculations and the corresponding mechanisms of the electrocatalytic HER on the surfaces of different catalysts under alkaline conditions. $\Delta G(H_2O)$ and ΔG(H) are the related kinetic energy barriers for the Volmer and Tafel steps on the catalysts, respectively. G(OH) is the Gibbs free energy of the adsorbed ^{-}OH on the surfaces of catalysts. E (eV) in the diagram represents the free energies of the different reactive stages. The yellow, blue and red spheres represent S, Mo and Ni, respectively.

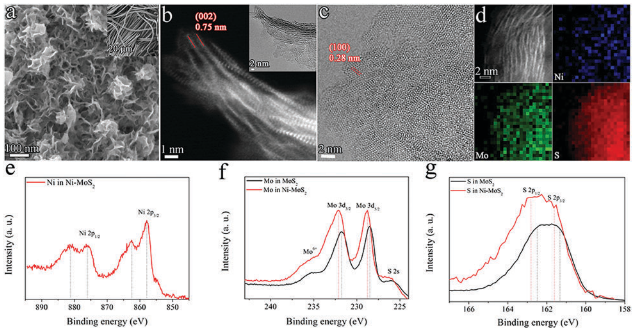

Fig. 2 Morphology and structural characterization of the Ni-MoS_2 catalysts. (a) SEM and (b and c) HRTEM images of the Ni-MoS_2 nanosheets; (d) corresponding STEM-EDS chemical mappings of Ni, Mo, and S elements in the Ni-MoS_2 nanosheets; high-resolution XPS spectra of (e) Ni 2p, (f) Mo 3d, and (g) S 2p in the MoS_2 and Ni-MoS_2 nanosheets. The insets in (a and b) are the low-magnification SEM image of the Ni-MoS_2 nanosheets coated on the carbon cloth and the HRTEM image of the edges of the Ni-MoS_2 nanosheets, respectively.

Open Access Article. Published on 19 July 2016. Downloaded on 9/12/2024 7:48:15 PM. This article is licensed under a Creative Commons Attribution-NonCommercial 3.0 Unported Licence.

field-emission SEM (FE-SEM) reveal the homogenous distributions of Ni, Mo, and S elements over the Ni-MoS_2 nanosheets (Fig. S5a–e, ESI†). The corresponding energy dispersive X-ray spectroscopy (EDS) analysis further suggests a chemical elemental composition of $Ni_{0.13}Mo_{0.87}S_2$ (Fig. S5f, ESI†). Fig. 2b and c show the HRTEM images of the Ni-MoS_2 nanosheets. Lattice fringes with lattice distances of 0.75 and 0.28 nm correspond to the (002) edge and (100) plane facets of the Ni-MoS_2 nanosheets, respectively.[16] Scanning TEM (STEM)-EDS characterization was utilized to analyze the elemental distributions in the Ni-MoS_2 nanosheets (Fig. 2d). Apparently, the Ni atoms are homogeneously distributed in the Ni-MoS_2 nanosheets. Similarly, the morphologies and chemical compositions of the as-prepared MoS_2, Co-MoS_2, and Fe-MoS_2 nanosheets were also investigated by SEM, XRD and EDS analyses (Fig. S6–S8, ESI†).

X-ray photoelectron spectroscopy (XPS) was applied to probe the composition and valence state of the Ni-MoS_2 nanosheets. The survey spectrum demonstrates a chemical composition of $Ni_{0.12}Mo_{0.88}S_2$, which is consistent with inductively coupled plasma mass spectrometry (ICP-MS) analysis ($Ni_{0.13}Mo_{0.87}S_2$) (Fig. S9–S11, ESI†). The peaks of Ni $2p_{3/2}$ and Ni $2p_{1/2}$ were observed at 857.9 eV and 876.0 eV, respectively (Fig. 2e). The binding energies of Mo $3d_{5/2}$ and Mo $3d_{3/2}$ in the Ni-MoS_2 nanosheets shifted to 228.8 and 232.1 eV, respectively (Fig. 2f), in contrast to those (Mo $3d_{5/2}$ at 228.5 and Mo $3d_{3/2}$ at 231.8 eV) in the pristine MoS_2 nanosheets. Likewise, the S $2p_{3/2}$ and S $2p_{1/2}$ signals in the Ni-MoS_2 also have a shift of ∼0.3 eV, relative to those in the MoS_2 nanosheets (Fig. 2g and Fig. S9, ESI†). Raman spectroscopy was further used to survey the Ni-MoS_2 nanosheets. The characteristic Raman bands of the A_{1g} and E^1_{2g} modes of Ni-MoS_2 shifted to 406 and 376 cm^{-1}, relative to the MoS_2 nanosheets (A_{1g} at 412 cm^{-1}; E^1_{2g} at 388 cm^{-1}) (Fig. S12, ESI†). These XPS and Raman results highlight the strong influence of Ni atom doping on the electronic structure of MoS_2.

To evaluate the electrocatalytic HER activities of the catalysts, a three-electrode configuration in Ar-saturated 1 M KOH aqueous solution was applied using a Hg/HgO electrode and a graphite rod as the reference and counter electrodes, respectively (Fig. S13, ESI†). All potentials are referenced to the reversible hydrogen electrode (RHE) and the ohmic potential drop caused by the solution resistance has been deducted unless noted (Fig. S14, ESI†). As shown in Fig. 3a, although MoS_2 can act as a HER catalyst, the hydrogen evolution reaction occurred at an overpotential of ∼197 mV and the cathodic current density reached 10 mA cm^{-2} at a high overpotential of ∼308 mV. Noticeably, the doping of Ni, Co, or Fe atoms into MoS_2 nanosheets leads to profound enhancements of the HER activities. Specifically, Co-MoS_2 and Fe-MoS_2 catalysts show overpotentials of only 203 and 163 mV at a current density of 10 mA cm^{-2}, respectively. Remarkably, the onset overpotential of Ni-MoS_2 catalysts was as low as 45 mV and a current density of 10 mA cm^{-2} was delivered at an extremely low overpotential of ∼98 mV, which is much lower than those of the as-prepared MoS_2 catalysts (∼308 mV at 10 mA cm^{-2}) and the reported MoS_2-based catalysts (regardless of whether in basic and acidic solutions) including amorphous MoS_x film (∼500 mV at 4 mA cm^{-2}),[10] MoS_2 nanoparticles grown on graphene (∼155 mV at 10 mA cm^{-2}),[17] defect-rich MoS_2 nanosheets (∼190 mV at 10 mA cm^{-2}),[9] double-gyroid mesoporous MoS_2 films (∼235 mV at 10 mA cm^{-2}),[7] Li-MoS_2 films (∼168 mV at 10 mA cm^{-2}),[18] and CoS_x/MoS_2 hybrids (∼220 mV at 5 mA cm^{-2})[12] (Table S2, ESI†). Moreover, the HER overpotential achieved by the Ni-MoS_2 catalysts is comparable to those of highly active NiO/Ni heterostructures (∼80 mV at 10 mA cm^{-2}),[19] CoP nanowires on carbon cloth (∼209 mV at 10 mA cm^{-2}),[20] porous MoC_x nano-octahedra (∼151 mV at 10 mA cm^{-2}),[21] cobalt–sulfide films (∼180 mV at 10 mA cm^{-2}),[22] and CoO/Co/N-doped carbon hybrids (∼232 mV at 10 mA cm^{-2})[23] (Table S3, ESI†).

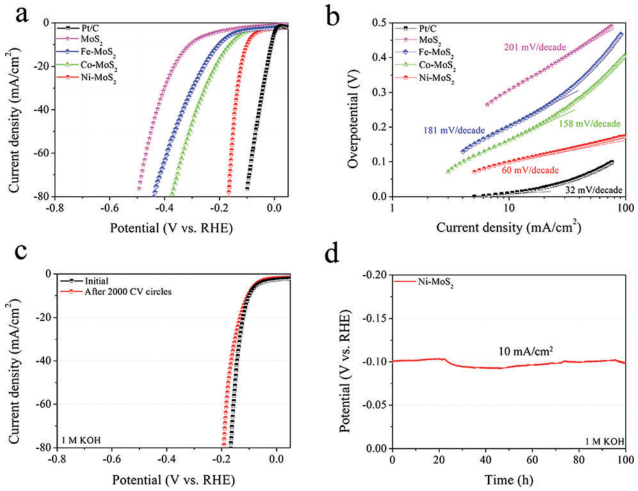

Fig. 3 Electrochemical HER measurements of different catalysts. (a) Polarization curves and (b) corresponding Tafel slopes of the MoS_2, Ni-MoS_2, Co-MoS_2, Fe-MoS_2, and commercial Pt/C catalysts; (c) CV stability and (d) 100 h operating durability of the Ni-MoS_2 catalysts in 1 M KOH aqueous solution. Scan rate: 1 mV s^{-1}.

Fig. 3b displays Tafel plots of the corresponding polarization curves, which provide further insights into the HER reaction pathways on the surfaces of the catalysts. The Tafel slope of the MoS_2 catalysts is as high as 201 mV per decade. However, the Tafel slope of the Ni-MoS_2 catalysts is significantly decreased to 60 mV per decade. Compared with the MoS_2 catalysts, the greatly decreased Tafel slope highlights that the kinetics of the water dissociation step is effectively facilitated on the Ni-MoS_2 catalysts. On the basis of the Tafel analysis, the exchange current density of the Ni-MoS_2 catalysts was estimated to be ∼0.98 mA cm^{-2} (Fig. S15, ESI†). Meanwhile, the turnover frequency (TOF) of the Ni-MoS_2 catalysts was up to 0.32 s^{-1} at an overpotential of 150 mV (Fig. S16, ESI†). In addition, the electrochemical impedance spectroscopy (EIS) analyses also confirmed a faster HER kinetic process on the Ni-MoS_2 catalysts than on the MoS_2 catalysts (Fig. S17, ESI†).

Electrocatalytic stability is another important criterion for the HER catalysts. For the Ni-MoS_2 catalysts, after 2000 cyclic voltammetry (CV) cycles in 1 M KOH aqueous solution, the overpotential required for a current density of 10 mA cm^{-2} increased by only 5 mV (Fig. 3c). A long-term HER process was

Open Access Article. Published on 19 July 2016. Downloaded on 9/12/2024 7:48:15 PM.
This article is licensed under a Creative Commons Attribution-NonCommercial 3.0 Unported Licence.

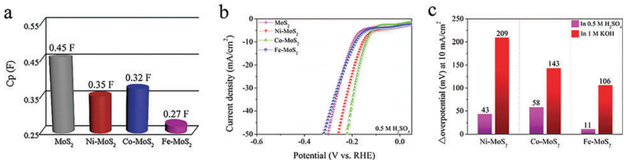

Fig. 4 (a) Electrochemical double layer capacitances of the as-achieved catalysts in 1 M KOH aqueous solution; (b) polarization curves of the catalysts in 0.5 M H_2SO_4 aqueous solution and (c) the alterations of the HER overpotentials of the catalysts under acidic and basic conditions.

performed at a current density of 10 mA cm^{-2} (Video S1, ESI†). Fig. 3d manifests that the Ni-MoS$_2$ catalysts retained a steady HER activity and no noticeable increase in potential was observed for hydrogen production over a period of 100 h. After the above HER durability assessment, the structural information of the Ni-MoS$_2$ catalysts was scrutinized using SEM. The morphology of the Ni-MoS$_2$ catalysts showed no structural variations, suggesting their superior structural stability during the HER process (Fig. S18, ESI†). The electrochemical stability of the Ni-MoS$_2$ catalysts was further confirmed by element mapping, EDX, and XPS analysis (Fig. S19 and S20, ESI†).

To clarify the influence of the active surface area on the electrocatalytic HER activity, the active surface areas of the as-synthesized catalysts were analyzed through their electrochemical double layer capacitances (C_p).[24] For comparison, the C_p of the MoS$_2$ catalysts was approximately 0.54 F. However, the Ni-MoS$_2$, Co-MoS$_2$, and Fe-MoS$_2$ catalysts showed low C_p values of ~0.35 F, 0.32 F, and 0.27 F, respectively (Fig. 4a and Fig. S21, ESI†). These results demonstrate that the excellent HER activity of the Ni-MoS$_2$ catalysts originates from the improved HER kinetics, rather than the active surface area. As illustrated in the reported volcano plots, under acidic conditions, the HER kinetics of a catalyst is strongly correlated with its hydrogen adsorption ability.[6,25] To further understand the roles of hydrogen adsorption and water dissociation in electrocatalytic HER kinetics of the Ni-MoS$_2$ catalysts, the electrochemical HER activities of the catalysts were tested under acidic conditions. As shown in Fig. 4b and c, in comparison with the MoS$_2$ catalysts, the HER overpotential of the Ni-MoS$_2$ catalysts at 10 mA cm^{-2} was decreased by only 43 mV in 0.5 M H_2SO_4 aqueous solution, which was far less than 209 mV in 1 M KOH aqueous solution. These studies clearly manifest that the greatly enhanced HER activity of the Ni-MoS$_2$ catalysts in 1 M KOH aqueous solution is mainly attributed to the initially accelerated water dissociation, rather than the hydrogen adsorption properties.

We also investigated a series of Ni-MoS$_2$ catalysts with different molar contents of Ni (Ni-MoS$_{2-x}$: x is expressed in Ni$_x$Mo$_{1-x}$S$_2$) in 1 M KOH aqueous solution (Fig. S22, ESI†). As shown in Fig. S23 (ESI†), the HER polarization curves of the Ni-MoS$_2$ catalysts dramatically shifted towards lower overpotentials along with the increased Ni content. When the molar content of Ni was ~13.3%, the Ni-MoS$_2$ catalysts exhibited the lowest HER overpotential (~98 mV at 10 mA cm^{-2}). The overpotential increased if the molar content of Ni was more than 13.3% and even the overpotential of the NiS$_2$ catalysts at 10 mA cm^{-2} was approximately 201 mV.

In summary, we have demonstrated a novel strategy to greatly accelerate the sluggish HER kinetics of MoS$_2$ electrocatalysts through engineering the water dissociation sites in alkaline environments. The combined DFT and experimental results show that the doping of Ni atoms into crystalline MoS$_2$ nanosheets can efficiently lower the kinetic energy barrier of the initial water dissociation step and facilitate the desorption of the formed $^{-}$OH from the surface of the Ni-MoS$_2$ catalysts. Therefore, this work opens up a favorable direction for exploring efficient and robust water-splitting catalysts, which have promising applications in alkali electrolyzers and solar-driven photocatalytic/photoelectrocatalytic devices.

Acknowledgements

This work was financially supported by an ERC grant on 2DMATER and EC under Graphene Flagship (No. CNECT-ICT-604391). We also acknowledge the Cfaed (Center for Advancing Electronics Dresden) and the Dresden Center for Nanoanalysis (DCN) at TU Dresden. P. L. and M. C. were supported by JST-CREST "Phase Interface Science for Highly Efficient Energy Utilization", Japan Science and Technology Agency.

Notes and references

1 N. S. Lewis and D. G. Nocera, *Proc. Natl. Acad. Sci. U. S. A.*, 2006, **103**, 15729.
2 K. Zeng and D. Zhang, *Prog. Energy Combust. Sci.*, 2010, **36**, 307; M. G. Walter, E. L. Warren, J. R. McKone, S. W. Boettcher, Q. Mi, E. A. Santori and N. S. Lewis, *Chem. Rev.*, 2010, **110**, 6446; J. S. Zhang, Y. Chen and X. C. Wang, *Energy Environ. Sci.*, 2015, **8**, 3092.
3 M. S. Faber and S. Jin, *Energy Environ. Sci.*, 2014, **7**, 3519; C. G. Morales-Guio, L.-A. Stern and X. Hu, *Chem. Soc. Rev.*, 2014, **43**, 6555.
4 X. Zou and Y. Zhang, *Chem. Soc. Rev.*, 2015, **44**, 5148; Y. Zheng, Y. Jiao, M. Jaroniec and S. Z. Qiao, *Angew. Chem., Int. Ed.*, 2015, **54**, 52.
5 X. Chia, A. Y. S. Eng, A. Ambrosi, S. M. Tan and M. Pumera, *Chem. Rev.*, 2015, **115**, 11941; Q. Lu, Y. Yu, Q. Ma, B. Chen and H. Zhang, *Adv. Mater.*, 2016, **28**, 1917; Y. D. Hou, A. B. Laursen, J. S. Zhang, G. G. Zhang, Y. S. Zhu, X. C. Wang, S. Dahl and I. Chorkendorff, *Angew. Chem., Int. Ed.*, 2013, **52**, 3621; G. Zhang, H. J. Liu, J. H. Qu and J. H. Li, *Energy Environ. Sci.*, 2016, **9**, 1190; X. W. Zhang, F. Meng, S. Mao, Q. Ding, M. J. Shearer, M. S. Faber, J. H. Chen, R. J. Hamers and S. Jin, *Energy Environ. Sci.*, 2015, **8**, 862.
6 B. Hinnemann, P. G. Moses, J. Bonde, K. P. Jørgensen, J. H. Nielsen, S. Horch, I. Chorkendorff and J. K. Nørskov, *J. Am. Chem. Soc.*, 2005, **127**, 5308; T. F. Jaramillo, K. P. Jørgensen, J. Bonde, J. H. Nielsen, S. Horch and I. Chorkendorff, *Science*, 2007, **317**, 100.
7 J. Kibsgaard, Z. Chen, B. N. Reinecke and T. F. Jaramillo, *Nat. Mater.*, 2012, **11**, 963.

This journal is © The Royal Society of Chemistry 2016

Open Access Article. Published on 19 July 2016. Downloaded on 9/12/2024 7:48:15 PM.
This article is licensed under a Creative Commons Attribution-NonCommercial 3.0 Unported Licence.

8 D. Kong, H. Wang, J. J. Cha, M. Pasta, K. J. Koski, J. Yao and Y. Cui, *Nano Lett.*, 2013, **13**, 1341.

9 J. Xie, H. Zhang, S. Li, R. Wang, X. Sun, M. Zhou, J. Zhou, X. W. Lou and Y. Xie, *Adv. Mater.*, 2013, **25**, 5807.

10 D. Merki, S. Fierro, H. Vrubel and X. Hu, *Chem. Sci.*, 2011, **2**, 1262.

11 J. Kibsgaard, T. F. Jaramillo and F. Besenbacher, *Nat. Chem.*, 2014, **6**, 248.

12 J. Staszak-Jirkovsky, C. D. Malliakas, P. P. Lopes, N. Danilovic, S. S. Kota, K.-C. Chang, B. Genorio, D. Strmcnik, V. R. Stamenkovic, M. G. Kanatzidis and N. M. Markovic, *Nat. Mater.*, 2015, **15**, 197.

13 R. Subbaraman, D. Tripkovic, D. Strmcnik, K.-C. Chang, M. Uchimura, A. P. Paulikas, V. Stamenkovic and N. M. Markovic, *Science*, 2011, **334**, 1256; R. Subbaraman, D. Tripkovic, K.-C. Chang, D. Strmcnik, A. P. Paulikas, P. Hirunsit, M. Chan, J. Greeley, V. Stamenkovic and N. M. Markovic, *Nat. Mater.*, 2012, **11**, 550.

14 D. J. Li, U. N. Maiti, J. Lim, D. S. Choi, W. J. Lee, Y. Oh, G. Y. Lee and S. O. Kim, *Nano Lett.*, 2014, **14**, 1228.

15 J. Zhang, S. Liu, H. Liang, R. Dong and X. Feng, *Adv. Mater.*, 2015, **27**, 7426.

16 J. Miao, F.-X. Xiao, H. B. Yang, S. Y. Khoo, J. Chen, Z. Fan, Y.-Y. Hsu, H. M. Chen, H. Zhang and B. Liu, *Sci. Adv.*, 2015, **1**, e1500259.

17 Y. Li, H. Wang, L. Xie, Y. Liang, G. Hong and H. Dai, *J. Am. Chem. Soc.*, 2011, **133**, 7296.

18 H. Wang, Z. Lu, S. Xu, D. Kong, J. J. Cha, G. Zheng, P.-C. Hsu, K. Yan, D. Bradshaw, F. B. Prinz and Y. Cui, *Proc. Natl. Acad. Sci. U. S. A.*, 2013, **110**, 19701.

19 M. Gong, W. Zhou, M.-C. Tsai, J. Zhou, M. Guan, M.-C. Lin, B. Zhang, Y. Hu, D.-Y. Wang, J. Yang, S. J. Pennycook, B.-J. Hwang and H. Dai, *Nat. Commun.*, 2014, **5**, 4695.

20 J. Tian, Q. Liu, A. M. Asiri and X. Sun, *J. Am. Chem. Soc.*, 2014, **136**, 7587.

21 H. B. Wu, B. Y. Xia, L. Yu, X.-Y. Yu and X. W. Lou, *Nat. Commun.*, 2015, **6**, 6512.

22 Y. Sun, C. Liu, D. C. Grauer, J. Yano, J. R. Long, P. Yang and C. J. Chang, *J. Am. Chem. Soc.*, 2013, **135**, 17699.

23 H. Jin, J. Wang, D. Su, Z. Wei, Z. Pang and Y. Wang, *J. Am. Chem. Soc.*, 2015, **137**, 2688.

24 M. A. Lukowski, A. S. Daniel, F. Meng, A. Forticaux, L. Li and S. Jin, *J. Am. Chem. Soc.*, 2013, **135**, 10274.

25 J. Greeley, T. F. Jaramillo, J. Bonde, I. Chorkendorff and J. K. Norskov, *Nat. Mater.*, 2006, **5**, 909.